Artificial phototropism for omnidirectional tracking and harvesting of light

Xiaoshi Qian [1,5], Yusen Zhao[1,5], Yousif Alsaid[1,5], Xu Wang[2], Mutian Hua[1], Tiphaine Galy[3], Hamsini Gopalakrishna [2], Yunyun Yang[1], Jinsong Cui[1], Ning Liu[1], Michal Marszewski [3], Laurent Pilon[3], Hanqing Jiang [2] and Ximin He [1,4]*

Many living organisms track light sources and halt their movement when alignment is achieved. This phenomenon, known as phototropism, occurs, for example, when plants self-orient to face the sun throughout the day. Although many artificial smart materials exhibit non-directional, nastic behaviour in response to an external stimulus, no synthetic material can intrinsically detect and accurately track the direction of the stimulus, that is, exhibit tropistic behaviour. Here we report an artificial phototropic system based on nanostructured stimuli-responsive polymers that can aim and align to the incident light direction in the three-dimensions over a broad temperature range. Such adaptive reconfiguration is realized through a built-in feedback loop rooted in the photothermal and mechanical properties of the material. This system is termed a sunflower-like biomimetic omnidirectional tracker (SunBOT). We show that an array of SunBOTs can, in principle, be used in solar vapour generation devices, as it achieves up to a 400% solar energy-harvesting enhancement over non-tropistic materials at oblique illumination angles. The principle behind our SunBOTs is universal and can be extended to many responsive materials and a broad range of stimuli.

Many living organisms present the unique capability of directionally moving towards sources of certain environmental stimuli. For example, cells and bacteria can migrate towards sources of chemical gradients, known as chemotaxis, for food (for example, glucose), fertilization (for example, sperm moving towards the egg) or immune functions[1]. Plants can self-orient to face light sources perpendicularly, known as phototropism (Fig. 1a), for energy harvesting and reproduction. All their direction of locomotion is strictly determined by the direction of an environmental stimulus, namely, tropistic movement, in contrast to nastic movement, which is a non-directional response to stimuli and simply determined by organism anatomy[2]. In tropistic movement, organisms not only sense and respond to the stimuli positions, but also spontaneously and constantly adjust their movements to tightly follow the signal directions. This presents the intelligence of self-regulation via the feedback control inherent in the dynamic interactions between their bodies and the stimulus.

Artificial materials, however, have not realized tropistic behaviours, in spite of many nastic behaviours presented with various stimuli-responsive materials that change volume or actuate on light, electrical or magnetic fields, pH or temperature changes[2]. For example, photoresponsive liquid crystalline elastomers bend under the light illumination[3]. However, the bending direction is determined by the anisotropic molecular orientation rather than the illumination direction and also varies with the ambient condition fluctuations (for example, temperature, light intensity and so on), which shows the lack of a robust movement-control mechanism. Recently, photoresponsive polymers were found capable of following the illumination direction in a non-steady oscillatory manner due to inertia[4–6]. However, achieving synthetic tropistic behaviour that can steadily track input energy has proved a daunting challenge[2,7]. Realizing

self-regulation in synthetic materials, such as in artificial homeostasis[8], requires a conceptually new broad-based design that owns a built-in feedback control to tightly regulate the multiple physics coupling and steadily rectify its resultant motion. Such self-adaptive, tropistic materials would be capable of a variety of plant-like autonomous motions and enable novel functions useful, for example, in soft robotics and automated systems.

Phototropism is developed by many plants as a strategy to recover the oblique-incidence energy-density loss (OEL), the input power density reduction when emissive energy projects on a surface obliquely. The loss can be enormous when the incident angle is large (for example, 75% loss at 75° incidence) (Fig. 1b). By maintaining normal incidence, sunflowers raise the temperature of floral discs to attract more pollinators with warmth and show an effective recovery of the input loss caused by oblique illumination if no phototropism was present[9]. Artificial phototropism, if realized, may provide an efficient solution to overcome this universal OEL issue faced by almost all existing optical and electromagnetic devices[10–13]. As a bioinspired concept illustrates in Fig. 1b, when a surface is covered with sunflower-like pillars that can bend towards the light source and maintain normal incidence, the original maximum power density ($P_{max} = P_0$) can be restored. The capability to harness tropistic behaviour autonomously, without external instruction and power supply (for example, via electromechanically programmed systems), would enable highly efficient energy-harvesting platforms that can adapt autonomously to complex ambient environments. However, current state-of-the-art photoactuations remain primarily nastic[14–18], unable to sense, track and harvest the emissive energy from varying incident directions self-adaptively.

Here we present a general principle of creating artificial phototropism with a series of reversibly photoresponsive polymers.

[1]Department of Material Science and Engineering, University of California Los Angeles, Los Angeles, CA, USA. [2]School for Engineering of Matter, Transport and Energy, Arizona State University, Tempe, AZ, USA. [3]Department of Mechanical and Aerospace Engineering, University of California Los Angeles, Los Angeles, CA, USA. [4]California Nanosystems Institute, Los Angeles, CA, USA. [5]These authors contributed equally: Xiaoshi Qian, Yusen Zhao, Yousif Alsaid. *e-mail: ximinhe@ucla.edu
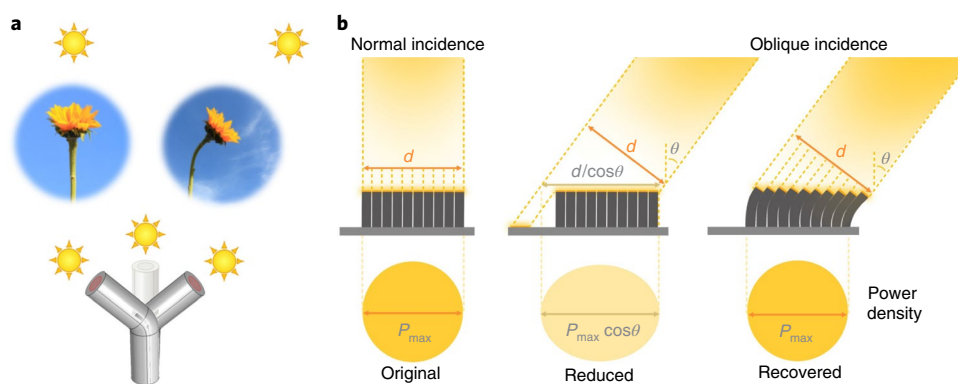
Fig. 1 | The concept of the artificial phototropism and the SunBOTs. a, Phototropism of sunflowers and the SunBOT. **b**, The concept of OEL recovery by phototropism. The OEL from P_{max} under the normal incidence (left) to $P_\theta = P_{max}\cos\theta$ under an oblique incidence at a θ zenith angle ($P_{max} = P_\theta$ ($\theta = 0°$)) suffered by a conventional non-phototropic surface (middle) can be fully recovered by a surface covered with a phototropic array (right).

These phototropic systems, termed sunflower-like biomimetic omnidirectional tracker (SunBOT) (Fig. 1a), can autonomously and instantaneously detect and track incident light in three-dimensional space at broad ambient temperatures with high accuracy and fast response, without auxiliary power supply or human intervention. We demonstrated that the artificial phototropism can achieve up to 400% energy-harvesting enhancement over conventional, non-tropistic materials under oblique illuminations. Owing to the broad choice of materials, tunable mechanics, and physical simplicity, the artificial phototropism is a broad-based platform, with potential impact in energy, robotics, and environmental applications.

Design principle and operation mechanism

Plants track light through photoreceptors in their stems that detect the incident light and lead to cell elongation on the shaded side, due to a distribution gradient of a growth factor (for example, auxin) between the illuminated and the shaded side[9]. To mimic the biological asymmetric growth, we leverage the capabilities of reversibly photothermoresponsive soft materials that shrink on illumination and adopt the symmetric stem-like cylindrical pillar shape for the design of SunBOTs. Like a stem, SunBOTs bend towards stimuli due to the asymmetric deformation between the illuminated high-temperature region and the shaded low-temperature region, as shown in Fig. 2f. SunBOT is a versatile platform that can be constructed using almost any reversibly photoresponsive soft materials, for example, hydrogels[8,14,19–22], liquid crystal elastomers (LCEs)[3,23,24] and azobenzene/spiropyran-based polymers[16,25]. Here we demonstrate the generality of the principle with four different photothermally responsive polymers. They are (1) a thermoresponsive hydrogel, poly(N-isopropylacrylamide) (PNIPAAm)[4,8,26], with homogeneously distributed nanophotoabsorbers, either gold nanoparticles (AuNPs) or reduced graphene oxide (rGO), which simultaneously act as photoreceptors and photothermal converters, respectively, termed AuNP–PNIPAAm SunBOTs (Figs. 2–4) and rGO–PNIPAAm SunBOTs (Fig. 5), (2) copolymerization of PNIPAAm and poly-acrylamide (PAM) with polypyrrole as the photoabsorber, termed a PAM-co-PNIPAAm SunBOT (Fig. 2c), (3) poly(2-dimethylamino) ethyl methacrylate (PDMAEMA) hydrogel with polyanaline (PANI) as the photoabsorber, termed a PANI–PDMAEMA SunBOT (Fig. 2b) and (4) LCE (Fig. 2d) specifically based on diacrylate mesogen RM257 with a homogeneously distributed indigo dye as the photoabsorber, termed an indigo–LCE SunBOT.

As Fig. 2a and Supplementary Videos 1–4 show, SunBOTs can adaptively reconfigure to follow and to orient themselves perpendicular to the incident light from arbitrary and constantly varying directions (−150 to 150° zenith, 360° azimuth) at room temperature.

This artificial phototropism capability achieves a remarkably high tracking accuracy (that is, the ratio of the pillar final bending angle and the light incident angle) of >99.8% (Fig. 2e), a fast response rate of 0.03 s deg^{-1} and up to a 400% energy-harvest enhancement.

Similar to sunflowers, the phototracking process of SunBOTs involves four steps: detection, actuation, aiming and recovery, as shown in Fig. 2f(i)–(iv). On illumination, the SunBOT detects the incident light via surface plasmon resonance of the incorporated nanophotoabsorbers (Fig. 2f(i)) and actuates towards the source due to local heating and asymmetric deformation (Fig. 2f(ii)). The asymmetric deformation is induced by establishing an appropriate temperature gradient across the pillar, where the illuminated front-side temperature (T_f) is greater than the hydrogel's lower critical solution temperature (LCST) and the shaded back-side temperature (T_b) remains below the LCST. This illuminated-side shrinkage results in a bending effect similar to that observed in plant stems. As soon as the SunBOT aims at the light source, it spontaneously terminates the actuation motion (Fig. 2f(iii)). The aiming as a self-regulated actuation is modulated by the negative feedback loop inherent in the tight hydrogel–stimuli interactions. As illustrated in Fig. 2g, localized exposure to the incident photonic energy results in a local shrinkage of the hydrogel and mechanical bending of the SunBOT pillar, which consequently blocks the light as an overshooting protection, allowing the hydrogel to reswell and repeat the cycles automatically, which results in a steady state of aiming. This self-shading effect is proved by the measured temperature evolution, as both T_f and T_b converge to be tightly around the LCST (Fig. 2h). Unlike previously reported nastic motions, which are sensitive to the intensity of the stimuli and/or the ambient temperature, the rigorous self-regulating mechanism generates similar temperature gradients in SunBOTs under different illumination powers and environment conditions (Supplementary Fig. 10), which guarantee a stable and accurate aiming at broad power and temperature ranges (Supplementary Section 2.4.2). When the illumination is turned off or changes position, the bent SunBOT immediately recovers its original shape or quickly adjusts its orientation to accommodate the position of a new stimulus (Fig. 2f(iv)), to perform another tropistic cycle in real time.

Overall, artificial phototropism is a self-regulatory effect that results from an elegant balance of the fully coupled participating physical processes: photothermal conversion, thermal diffusion, mass (water) diffusion and mechanical deformation. Comprehensive theoretical efforts, specifically a multiphysics model that couples the light, heat, mass transfer and mechanics across nano-to-millimetre scales, have been developed to understand the fundamentals of the phototropic process and to guide the rational design predictively (Supplementary Section 4).
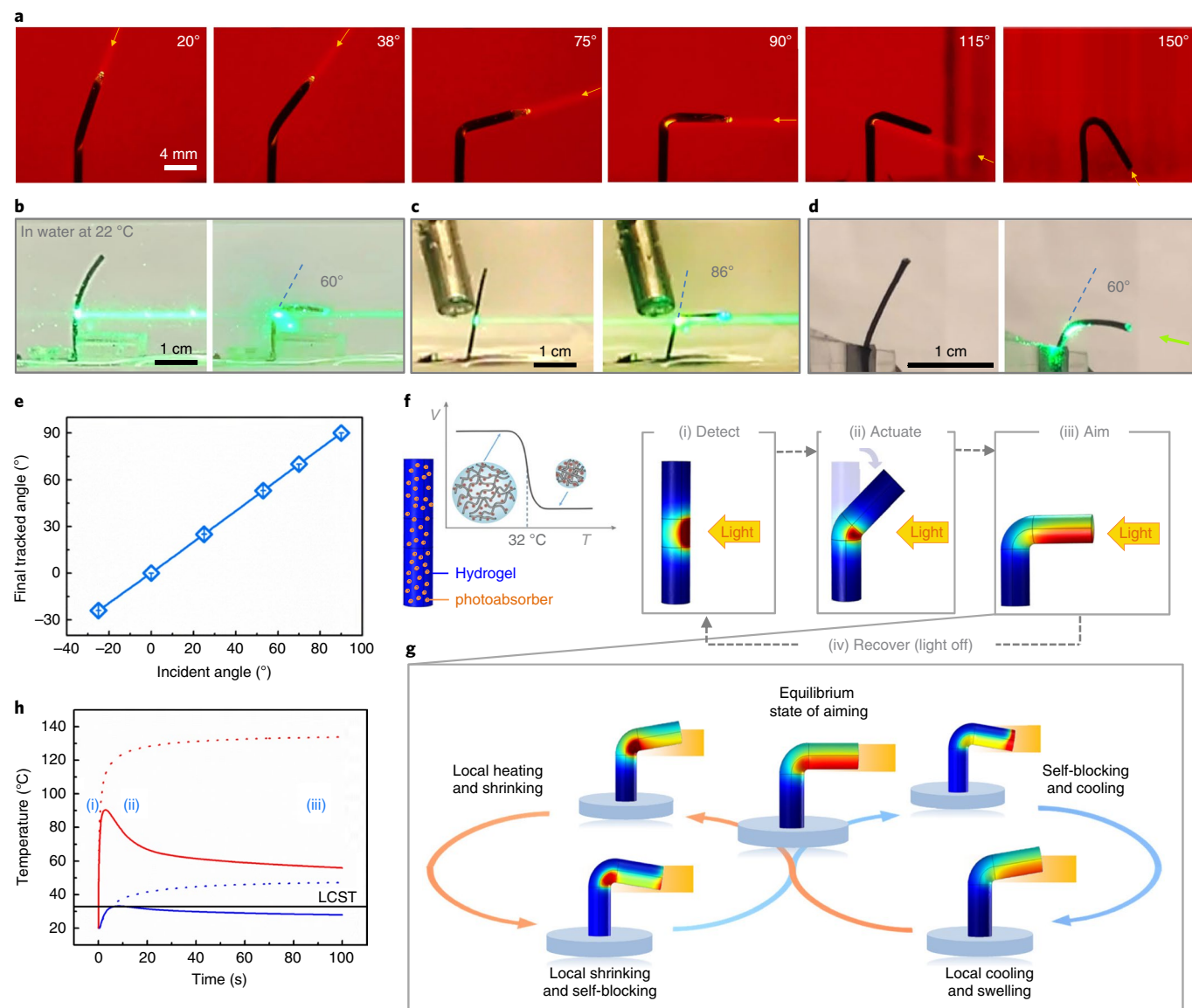
Fig. 2 | The design and mechanism of SunBOTs. a, Photos of an AuNP–PNIPAAm SunBOT in water aiming at a laser that illuminates from various zenith angles in the range 20–150°. **b–d**, Photos of the phototropic movement of SunBOTs based on PANI–PDMAEMA in water at 22 °C (**b**), PAM-co-PNIPAAm in water at 70 °C (**c**) and indigo–LCE in air (**d**). **e**, The SunBOT aims towards the light source with a high tracking accuracy (<0.2% error). **f**, SunBOT design and phototropic mechanism. Inset: the volume (*V*) versus temperature (*T*) plot demonstrates PNIPAAm hydrogel's thermally responsive behaviour with a LCST around 32 °C, which is tunable as shown in **c**. **g**, The equilibrium state of aiming is regulated by a built-in negative feedback loop with self-blocking capability. **h**, The temperature evolution during steps (i)–(iii) in **f** shows that the temperatures at the illuminated front side (red) and the shaded back side (blue) of the SunBOT are self-regulated due to the self-blocking and converge to be tightly above and below the LCST (black line), in contrast to the non-regulated temperatures with a lack of self-blocking (dotted lines).

Operation performance of tracking

The simulated thermal and stretch fields within the SunBOT pillar (Fig. 3b,c) reveal that this wide-angle tracking ability is induced primarily by contraction at the illuminated region rather than governed by the material stiffness or flexural modulus, as in typical elastic beam bending (Supplementary Section 2.5). This mechanics further highlights the freedom in material selection. Moreover, the phototropism of SunBOTs is energy efficient. As this light-powered hydrogel reconfiguration is essentially a volumetric phase transition with a tunable LCST[27], it consumes a minute amount of photonic power to locally heat the hydrogel and trigger the release of a large amount of mechanical energy for the phase transition (Supplementary Section 2.6).

The SunBOT has a truly broad and tunable operation window that can guarantee successful phototropism over a wide range of light intensities (Fig. 3h, Supplementary Fig. 16 and Supplementary Table 1), ambient temperatures (Supplementary Fig. 15), lighting conditions (Fig. 3a–f), irregular geometric shapes (Fig. 3g) and spatiotemporal rhythms of illumination (Fig. 3i). These can be achieved by tuning the material properties, including the nanophotoabsorber concentration, transition temperature, dimension of the material and the coupling between the properties (Supplementary Section 2.4). Figure 3 presents the versatility of SunBOTs through more-complex direction-cognitive behaviours under various conditions. The SunBOT can track not only a spot light but also large-area lighting (Fig. 3a–f and Supplementary Video 5), which shows
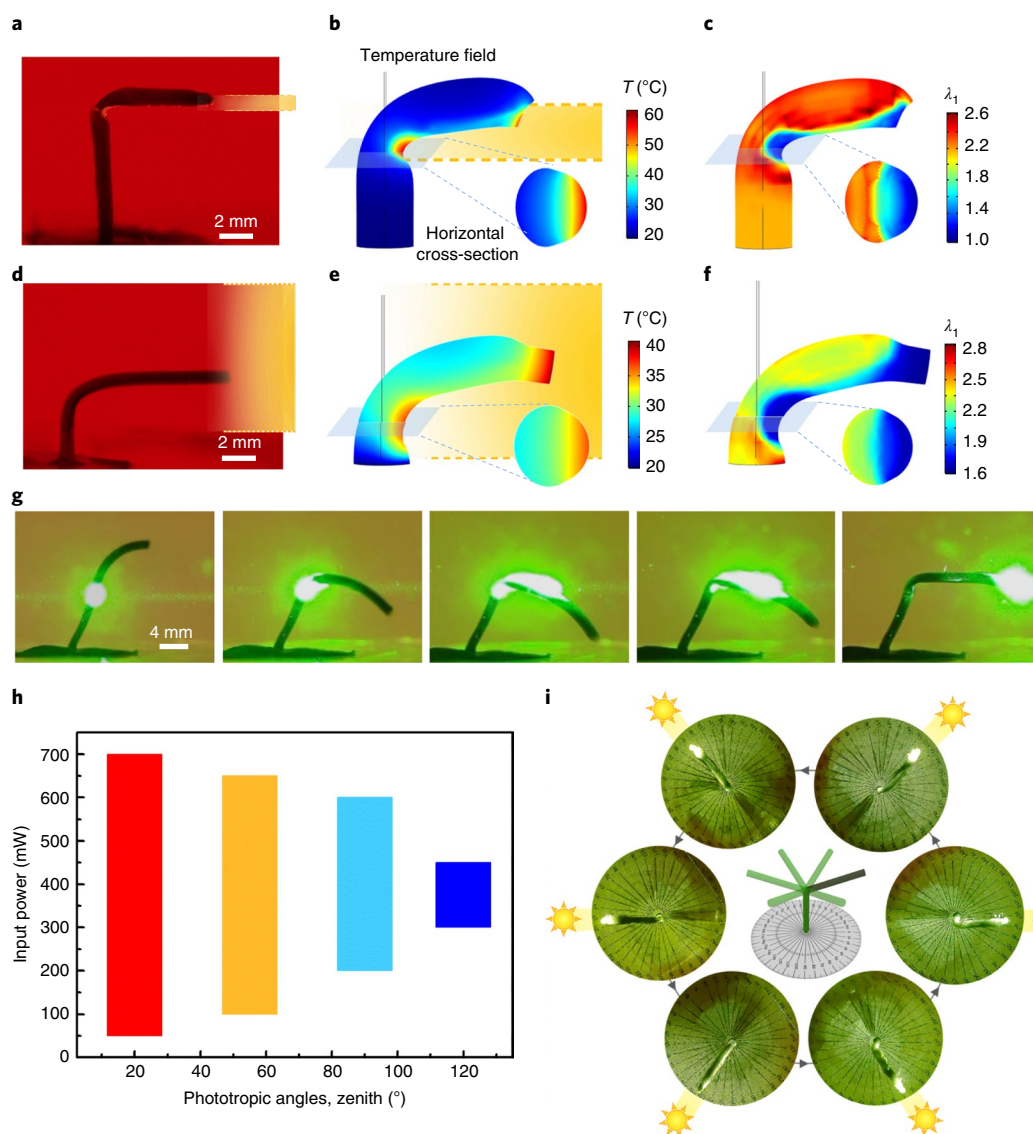
Fig. 3 | Complex and robust phototropic behaviours of SunBOTs. a–f, The SunBOT can track both a spotlight (1 mm beam width) (**a–c**) and an area light (20 mm beam width) (**d–f**), which exhibit different curvatures. The simulated temperature distribution (T) (**b** and **e**) and stretch field (λ_1, primary stretch in the 1-direction; at a fully dried state, $\lambda_1 = 1$) (**c** and **f**) of the steady aiming state captured the experimental results (**a** and **d**). Insets: cross-sections at the illumination sites. **g,** Snapshots of the process of an irregular-shaped SunBOT being straightened after bending (from left to right), which demonstrates the self-correction ability of a robust artificial phototropism. **h,** The operation windows of input power to successfully track the light of different incident angles (20–120° zenith). An input power smaller than the coloured histogram is not sufficient to allow the pillar to achieve phototracking. **i,** Top-view snapshots of a SunBOT continuously tracking light that revolves azimuthally around the SunBOT.

its applicability to ambient light conditions. The optical beam width can also effectively manipulate bending curvatures, which are accurately reproduced by multiphysics modelling (Supplementary Fig. 34). Interestingly, SunBOTs with arbitrary contorted pillar shapes can be straightened by the light (Fig. 3g, Supplementary Video 6 and Supplementary Fig. 17). Such high-fidelity tropism presents adaptive learning and self-optimization through continuous dynamic light–matter interactions. Ultimately, attributed to the fast recovery (reswelling) of the hydrogel when not being illuminated, the SunBOT can successfully track a light source in real time, continuously moving 360° azimuthally at a fast speed up to 0.03 s deg⁻¹ (Fig. 3i and Supplementary Video 3). At these intentionally designed pausing steps, the fast-moving SunBOT precisely stops at the light-source direction without any over- or underbending, which confirms an extremely strict spatiotemporal control

of the tracking behaviour by the light (Supplementary Fig. 8). Being both compositionally and geometrically symmetric, the design simplicity of SunBOTs endows them an infinite degree of freedom to fulfil a truly omnidirectional tracking and energy harvesting (Fig. 2a).

Kinetics study of the SunBOT
How fast a SunBOT can track the directional variation of the emissive energy is directly correlated to the ability to aim at the moving light source and hence the final energy production. Based on steady-state studies, we further investigated the kinetics of the dynamic tropistic locomotion, which was jointly determined by the thermal diffusion and the mass (water) diffusion. The timescale associated with thermal diffusion in the hydrogel remained the same during the deformation (Supplementary Section 2.4.3) and its dynamics were
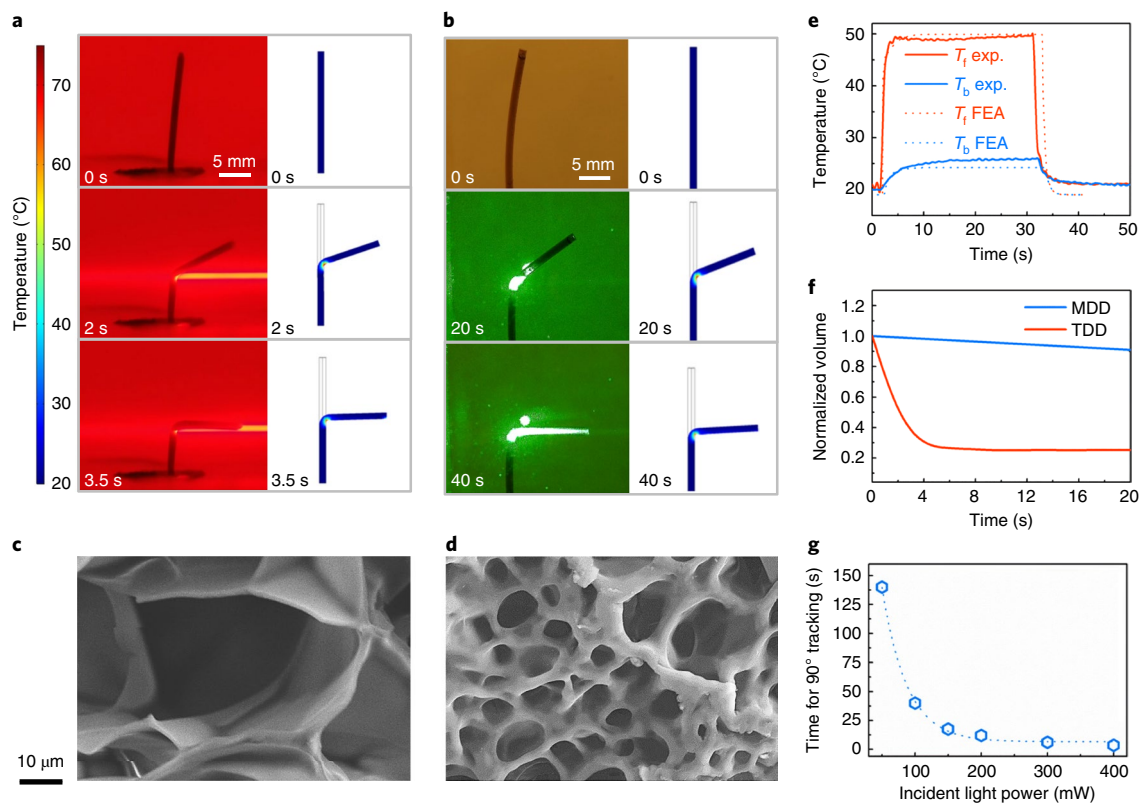
Fig. 4 | The tracking kinetics of the SunBOT. a, The kinetics of a TDD tracking process, evaluated by experiment (left) and finite element analysis (FEA) simulation (right), which synced perfectly. **b**, The kinetics of a MDD tracking process. Temperature scale applies to both **a** and **b**. **c,d**, Scanning electron microscopy images of PNIPAAm hydrogels used in the TDD SunBOTs with a 50 μm pore size (**c**) and in the MDD SunBOTs with a 5–10 μm pore size (**d**). **e**, The experimental (exp) and simulation results of T_f and T_b of the TDD SunBOTs under a 30 s illumination. **f**, A kinetics study of the thermal shrinkage of the hydrogels used in MDD and TDD SunBOTs. **g**, The time used to achieve 90° tracking at different incident light powers.

simulated in the multiphysics modelling (Fig. 4 and Supplementary Video 2). However, the mass diffusion can be manipulated by controlling the nano/microstructure of the hydrogel. Figure 4a,b exhibit distinct phototropic kinetics with different diffusion-dominated mechanisms. When the mass diffusion is relatively fast, that is, the water diffusion in the hydrogel matrix is completed by the time the steady-state temperature gradient is established, the tracking speed is limited by the thermal diffusion, and the SunBOT is thermal-diffusion dominated (TDD). As shown in Fig. 4a, the TDD SunBOT can track to 90° within 3.5 seconds (much faster than its natural counterparts), which is comparable to the time required to reach the thermal steady state (Fig. 4c). By contrast, the mass-diffusion dominated (MDD) SunBOT has much smaller pore sizes (Fig. 4d), and hence a much slower water diffusion. Consequently, it takes a longer time to reach a 90° tracking than that for the TDD SunBOT (Fig. 4b). To better understand these dynamic phototropic behaviours, we studied the temporal evolution of temperatures T_f and T_b near the incident site of the SunBOT experimentally and numerically (Fig. 4e). With the quantitative agreement between simulation and experimental results of the kinetic studies shown in Fig. 4a,b,e and Supplementary Video 2, we validated our numerical model, which applies the recorded dynamic swelling ratio of the hydrogel (Fig. 4f) to fit the mass diffusivity. The validation enabled a rational design and dynamic behaviour prediction by providing a comprehensive insight and clear physical picture of the fundamental mechanism.

As the microstructure of the hydrogel matrix provides a flexible tunability of the phototropic kinetics that the SunBOT achieves once the material system has been fabricated, one can still readily control its temporal response by varying the incident light power (Fig. 4g). The time cost of the successful 90° tracking of the SunBOT varies from hundreds of seconds to seconds, as long as the input power falls into the operation window discussed above.

Artificial phototropism enhanced energy harvesting

Ultimately, we demonstrated the efficacy of SunBOTs in solving practical OEL problems (Fig. 1b) by applying an array of micro-SunBOTs (500 μm diameter with a pitch of 1 mm) in solar energy harvesting. The micro-SunBOT array that incorporates rGO as a broadband photoabsorber can successfully track white-light incidence from the entire hemispheric space. This further demonstrated that the modular design can accommodate either single-wavelength or broad-spectrum light sources. Owing to the phototropism, the tips of the micro-SunBOT fibrils always received the maximum photonic power density (Fig. 5a–c) and thus compensated for the OEL. Comparing with a non-tropistic textured surface as the control sample (Supplementary Fig. 22), we evaluated the benefits of the tropistic oblique-loss compensation (OLC) enabled by the SunBOT.

By keeping the SunBOT array at the water–air interface under variable-angle illumination, which serves as a phototropic solar vapour generation (SVG) system, we evaluated the angle-dependent performances of the photonic energy absorption and conversion by measuring the generated water vapour mass flux (G_θ, the mass of vapour produced per unit area per unit time at incident angle θ). The area used to characterize $\bar{G}_\theta$ is the effective area of the SVG device, that is, the area positioned at the water–air interface and contributing to vapour generation due to the localized heating at the interface (Supplementary Section 3.2). To exclude the contribution to the vapour generation from the photothermal energy produced
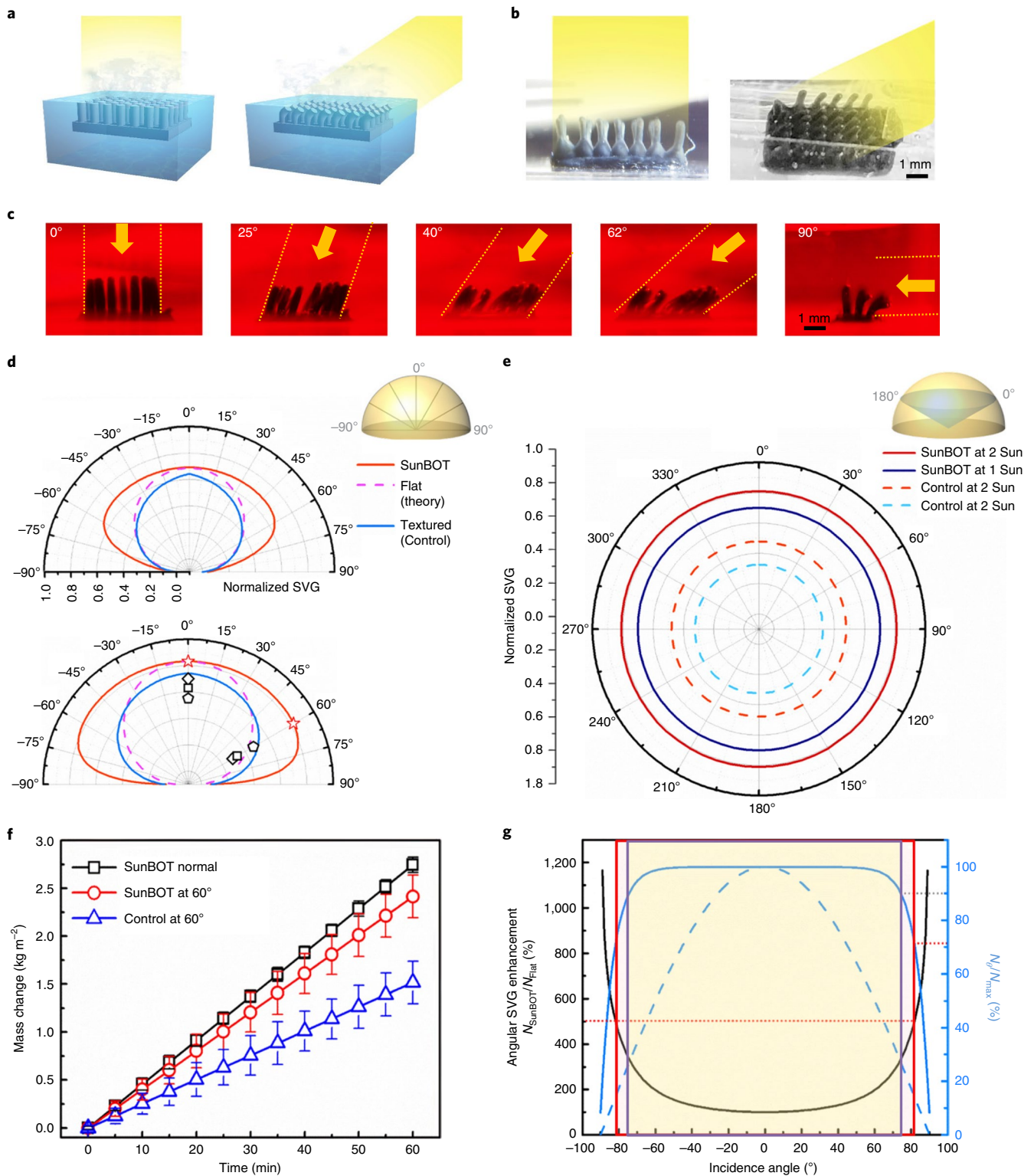
Fig. 5 | A demonstration of the energy maximization function of phototropism: OLC in the SVG. a,b, Schematic (**a**) and photos (**b**) of OLC in SVG, with a micro-SunBOT array that maximizes the white-light power density. **c**, Side-view photos of the micro-SunBOT array tracking various angles of incidence light (0–90°). **d**, The measured normalized SVG of SunBOT (rGO) under 1 Sun (top) and 2 Sun (bottom) illumination at various zenith angles from −90 to 90°, in comparison to control samples of a flat surface (in theory) and a non-tropistic textured surface and to previously reported SVG systems (diamond, Camacho-Lopez et al.[18]; square, Shastri et al.[19]; pentagon, Qin et al.[20]; star, this work). **e**, The SVG of a SunBOT (rGO) array under illumination from 0 to 360° azimuthal angles (zenith angle = 60°). **f**, Time-dependent SVG mass change per unit area by SunBOT(rGO) under a 60° (zenith) illumination is comparable to that under normal incidence, whereas the control sample exhibits a 45% reduction in SVG. Plots are centred on the mean and the bars indicate the s.d. **g**, The angle-dependent SVG of a SunBOT (blue solid line) and a flat surface (blue dashed line) and the enhancement ratio that compares the two (black curve), where N_θ is the normalized SVG under the light of an incident angle θ. The red and purple frames indicate two exemplary operation-angle windows with >75% and >90%, respectively, of the input energy density harvested.

by water (thermal mass) under illumination, G_θ has the baseline subtracted. The baseline was measured by recording the evaporation rate of a water bath with a total area equivalent to the total footprint of the SunBOT sample (including the pillar top and gap areas) under the same illuminating power but without the SunBOT. For a non-tropistic surface, the angle-dependent input photonic power density $P_\theta = P_{max}\cos\theta$ decreases as incident angle (θ) increases (Fig. 1b). This work focuses on studying the angle dependency of the energy harvesting by maximizing the input power density instead of the absolute SVG efficiency (Supplementary Section 3.2). Hence, we evaluated the phototropism-enabled OLC by defining a dimensionless value derived from G_θ, the normalized SVG ($N = G_\theta h_{LV}/(P_{max}C_{opt})$), where h_{LV} is the specific enthalpy of water vaporization ($J\,kg^{-1}$), C_{opt} is the optic concentration, which uses the constant photonic power density at normal incidence $P_{max} = P_\theta(\theta = 0°) = 1\,kW\,m^{-2}$ as the normalizing factor, instead of an angle-dependent P_θ. Under normal incidence, the normalized SVG degenerates to the efficiencies regularly defined in other previously reported SVG studies[28–30] (mostly under normal illumination).

When $\theta = 0°$, the SunBOT exhibited an SVG efficiency of 70% under a 1 Sun illumination and 80% under a 2 Sun illumination, which are comparable to the previously reported values[28–35]. When $\theta = 60°$ ($P_{60°} = 50\% P_{max}$), for non-tropistic surfaces the vapour flux G_θ reduced to 50% of $G_{\theta=0°}$. By contrast, the SunBOT array maintained 90% of $G_{\theta=0°}$ under normal incidence, which compensated the lost 40% of the input (Fig. 5f). Under 1 Sun and 2 Sun illuminations, the SunBOT phototropic SVG outperformed the control samples (Supplementary Section 3.1) at all incident angles (zenith and azimuth) in the entire hemisphere (Fig. 5d,e). At 60° (zenith), the phototropic SunBOT generated an SVG double that of a theoretical flat surface, the control samples and previous reports (Supplementary Section 3.2). The SunBOTs showed an omnidirectional SVG, which is defined as generating >90% of the maximum SVG ($\theta = 0°$) under oblique incidence, over a wide operation window of angles, that is, −60 to 60° for 1 Sun and −75 to 75° for 2 Sun, in contrast to the drastic reduction in both the theoretical estimation and control samples. In addition, the SunBOT array demonstrates an up to 400% enhancement (fivefold) of SVG with an operation window of 164° (−82 to 82°) (Fig. 5g). With varying incident angles daily and seasonally, the energy-harvesting enhancement on different seasonal days and throughout the time of year at different latitudes in the world are demonstrated in Supplementary Figs. 27–30 and Supplementary Section 3.3.4. For example, at the latitude of the Los Angeles area in the United States, the SunBOTs can theoretically improve the annual SVG by 165–200% compared to that of a flat surface at the same latitude, which recovers up to 77% of the lost solar power density due to the oblique illumination (Supplementary Fig. 30 and Supplementary Table 2). From the equator to high-latitude (60° N and 60° S) locations, where the majority of the population live, SunBOT is predicted to harvest 1.3–2.1 times more solar energy compared to a non-tropistic surface on equinox days (Supplementary Figs. 27 and 28).

Conclusions

We report here a synthetic phototropism via a sunflower-inspired, self-adaptive reconfigurable material system with a built-in feedback loop. The phototropic material features an omnidirectional self-orienting capability, in contrast to other actuating systems for energy harvesting that are typically made of uncontrollable or preprogrammed systems. Our experimental and numerical investigation generates new insight into the mechanism behind the plant-like phototropic motion, and also establishes a predictive model to guarantee a high fidelity and energy efficiency in the harvesting of broad forms of energy. The numerical framework that can couple a large number of physical fields provides a powerful tool to study our systems in depth. The SunBOTs exhibit biological sensorimotor-like

behaviour, controlled by a feedback loop inherent in the intricately coupled photochemomechanical interactions. This behaviour mimics the elegant agility of living systems, which leads to novel intelligent materials. Practically, our SunBOTs provide a long-sought solution to energy harvesting via the autonomous maximization of the input power density. The nearly infinite degree of freedom in their adaptive locomotion may lead to self-sustained, untethered soft robots[36], autonomously capable of real-time learning and performing complex tasks in various environments[37,38]. This work may be useful for enhanced solar harvesters[28–30], adaptive signal receivers[39], smart windows[40,41], self-contained robotics[42,43], solar sails for spaceships[44,45], guided surgery, self-regulating optical devices[46,47] and intelligent energy generation (for example, solar cells and biofuels[48]), as well as energetic emission detection and tracking with telescopes, radars and hydrophones.

Online content

References

1. Delves, P. J. & Roitt, I. M. Ivan M. *Encyclopedia of Immunology* (Academic, 1998).
2. Poppinga, S. et al. Toward a new generation of smart biomimetic actuators for architecture. *Adv. Mater.* **30**, 1703653 (2018).
3. White, T. J. & Broer, D. J. Programmable and adaptive mechanics with liquid crystal polymer networks and elastomers. *Nat. Mater.* **14**, 1087–1098 (2015).
4. Zhao, Y. et al. Soft phototactic swimmer based on self-sustained hydrogel oscillator. *Sci. Robot.* **4**, eaax7112 (2019).
5. Serak, S. et al. Liquid crystalline polymer cantilever oscillators fueled by light. *Soft Matter* **6**, 779–783 (2010).
6. Gelebart, A. H., Vantomme, G., Meijer, E. W. & Broer, D. J. Mastering the photothermal effect in liquid crystal networks: a general approach for self-sustained mechanical oscillators. *Adv. Mater.* **29**, 1606712 (2017).
7. Li, C., Liu, Y., Huang, X. & Jiang, H. Direct sun-driven artificial heliotropism for solar energy harvesting based on a photo-thermomechanical liquid–crystal elastomer nanocomposite. *Adv. Funct. Mater.* **22**, 5166–5174 (2012).
8. He, X. et al. Synthetic homeostatic materials with chemo-mechano-chemical self-regulation. *Nature* **487**, 214–218 (2012).
9. Atamian, H. S. et al. Circadian regulation of sunflower heliotropism, floral orientation, and pollinator visits. *Science* **353**, 587–590 (2016).
10. Greffet, J.-J. et al. Coherent emission of light by thermal sources. *Nature* **416**, 61–64 (2002).
11. Fink, Y. et al. A dielectric omnidirectional reflector. *Science* **282**, 1679–82 (1998).
12. Teperik, T. V. et al. Omnidirectional absorption in nanostructured metal surfaces. *Nat. Photon.* **2**, 299–301 (2008).
13. Huang, J. et al. Harnessing structural darkness in the visible and infrared wavelengths for a new source of light. *Nat. Nanotechnol.* **11**, 60–66 (2015).
14. Wang, E., Desai, M. S. & Lee, S.-W. Light-controlled graphene–elastin composite hydrogel actuators. *Nano Lett.* **13**, 2826–2830 (2013).
15. Ahir, S. V. & Terentjev, E. M. Photomechanical actuation in polymer–nanotube composites. *Nat. Mater.* **4**, 491–495 (2005).
16. Zhao, Y. L. & Fraser Stoddart, J. Azobenzene-based light-responsive hydrogel system. *Langmuir* **25**, 8442–8446 (2009).
17. Liu, X. et al. Reversible and rapid laser actuation of liquid crystalline elastomer micropillars with inclusion of gold nanoparticles. *Adv. Funct. Mater.* **25**, 3022–3032 (2015).
18. Camacho-Lopez, M., Finkelmann, H., Palffy-Muhoray, P. & Shelley, M. Fast liquid–crystal elastomer swims into the dark. *Nat. Mater.* **3**, 307–310 (2004).
19. Shastri, A. et al. An aptamer-functionalized chemomechanically modulated biomolecule catch-and-release system. *Nat. Chem.* **7**, 447–454 (2015).
20. Qin, M. et al. Bioinspired hydrogel interferometer for adaptive coloration and chemical sensing. *Adv. Mater.* **30**, 1800468 (2018).
21. Sun, M. et al. Hydrogel interferometry for ultrasensitive and highly selective chemical detection. *Adv. Mater.* **30**, 1804916 (2018).

22. Qin, M., Sun, M., Hua, M. & He, X. Bioinspired structural color sensors based on responsive soft materials. *Curr. Opin. Solid State Mater. Sci.* **23**, 13–27 (2019).

23. Gelebart, A. H. et al. Making waves in a photoactive polymer film. *Nature* **546**, 632–636 (2017).

24. Wani, O. M., Zeng, H. & Priimagi, A. A light-driven artificial flytrap. *Nat. Commun.* **8**, 15546 (2017).

25. Klajn, R. Spiropyran-based dynamic materials. *Chem. Soc. Rev.* **43**, 148–184 (2014).

26. Schild, H. G. Poly(*N*-isopropylacrylamide): experiment, theory and application. *Prog. Polym. Sci.* **17**, 163–249 (1992).

27. Taylor, L. D. & Cerankowski, L. D. Preparation of films exhibiting a balanced temperature dependence to permeation by aqueous solutions—a study of lower consolute behavior. *J. Polym. Sci. Polym. Chem. Ed.* **13**, 2551–2570 (1975).

28. Zhou, L. et al. 3D self-assembly of aluminium nanoparticles for plasmon-enhanced solar desalination. *Nat. Photonics* **10**, 393–398 (2016).

29. Ghasemi, H. et al. Solar steam generation by heat localization. *Nat. Commun.* **5**, 4449 (2014).

30. Zhao, F. et al. Highly efficient solar vapour generation via hierarchically nanostructured gels. *Nat. Nanotechnol.* **13**, 489–495 (2018).

31. Li, X. et al. Graphene oxide-based efficient and scalable solar desalination under one Sun with a confined 2D water path. *Proc. Natl Acad. Sci. USA* **113**, 13953–13958 (2016).

32. Zhou, L. et al. Self-assembled spectrum selective plasmonic absorbers with tunable bandwidth for solar energy conversion. *Nano Energy* **32**, 195–200 (2017).

33. Chen, Q. et al. A durable monolithic polymer foam for efficient solar steam generation. *Chem. Sci.* **9**, 623–628 (2018).

34. Wang, Y., Zhang, L. & Wang, P. Self-floating carbon nanotube membrane on macroporous silica substrate for highly efficient solar-driven interfacial water evaporation. *ACS Sustain. Chem. Eng.* **4**, 1223–1230 (2016).

35. Wang, Z. et al. Bio-inspired evaporation through plasmonic film of nanoparticles at the air–water interface. *Small* **10**, 3234–3239 (2014).

36. Donald, B. R., Levey, C. G., McGray, C. D., Paprotny, I. & Rus, D. An untethered, electrostatic, globally controllable MEMS micro-robot. *J. Microelectromech. Syst.* **15**, 1–15 (2006).

37. Liu, Q., Nian, G., Yang, C., Qu, S. & Suo, Z. Bonding dissimilar polymer networks in various manufacturing processes. *Nat. Commun.* **9**, 846 (2018).

38. Le Floch, P. et al. Wearable and washable conductors for active textiles. *ACS Appl. Mater. Interfaces* **9**, 25542–25552 (2017).

39. Hum, S. V. & Perruisseau-Carrier, J. Reconfigurable reflect arrays and array lenses for dynamic antenna beam control: a review. *IEEE Trans. Antennas Propag.* **62**, 183–198 (2014).

40. Zhu, M. et al. Transparent and haze wood composites for highly efficient broadband light management in solar cells. *Nano Energy* **26**, 332–339 (2016).

41. Li, T. et al. Wood composite as an energy efficient building material: guided sunlight transmittance and effective thermal insulation. *Adv. Energy Mater.* **6**, 1601122 (2016).

42. Zeng, H., Wasylczyk, P., Wiersma, D. S. & Priimagi, A. Light robots: bridging the gap between microrobotics and photomechanics in soft materials. *Adv. Mater.* **30**, e1703554 (2018).

43. Kim, Y., Yuk, H., Zhao, R., Chester, S. A. & Zhao, X. Printing ferromagnetic domains for untethered fast-transforming soft materials. *Nature* **558**, 274–279 (2018).

44. Costanza, G. & Tata, M. E. A novel methodology for solar sail opening employing shape memory alloy elements. *J. Intell. Mater. Syst. Struct.* **29**, 1793–1798 (2018).

45. Ullery, D. C. et al. Strong solar radiation forces from anomalously reflecting metasurfaces for solar sail attitude control. *Sci. Rep.* **8**, 10026 (2018).

46. Gelebart, A. H., Mc Bride, M., Schenning, A. P. H. J., Bowman, C. N. & Broer, D. J. Photoresponsive fiber array: toward mimicking the collective motion of cilia for transport applications. *Adv. Funct. Mater.* **26**, 5322–5327 (2016).

47. Yao, Y. et al. Electrically tunable metasurface perfect absorbers for ultrathin mid-infrared optical modulators. *Nano Lett.* **14**, 6526–6532 (2014).

48. Lee, E., Heng, R.-L. & Pilon, L. Spectral optical properties of selected photosynthetic microalgae producing biofuels. *J. Quant. Spectrosc. Radiat. Transf.* **114**, 122–135 (2013).

Methods

Fabrication of SunBOTs. The PNIPAAm hydrogel precursor solution was prepared with a 40 wt% NIPAAM monomer, 2 wt% crosslinker *N,N'*-methylenebisacrylamide, 0.5 vol% ultraviolet-initiator Darocur 1173 in dimethylsulfoxide (DMSO), followed by adding photoabsorbers AuNPs or rGO to fabricate SunBOTs based on AuNP–PNIPAAm or rGO–PNIPAAm, respectively. For the AuNP-incorporated SunBOT (AuNP–SunBOT), 0.8 wt% AuNPs and 0.1 vol% allyl disulfide (optional, used in MDD SunBOTs only and not used in TDD SunBOTs (Supplementary Section 1.3.1)) were added into the PNIPAAm precursor solution in DMSO, in which the allyl disulfide serves as a linker between the AuNPs and hydrogel matrix via hydrogen bonds. For the rGO-incorporated SunBOT (rGO–SunBOT), 0.3 wt% rGO was added to the PNIPAAm precursor solution in DMSO. The mixture solution was then poured into the polydimethylsiloxane mould and covered with a 3-(trimethoxysilyl)propyl methacrylate-treated glass slide, followed by ultraviolet curing for 60 s. The cured gel structure was carefully pulled out from the mould to yield a SunBOT, and then immersed into deionized water to remove DMSO. For the rGO–SunBOTs, the gel structure was soaked in a 0.33 M hydrazine aqueous solution to reduce the graphene oxide to rGO. If not specifically identified, the fully hydrated SunBOT (single pillar) had a diameter of 1 mm and a length of 10–20 mm at room temperature; each fully hydrated pillar in the SunBOT arrays had a diameter of 0.5 mm at room temperature.

Characterization of the artificial phototropism. A 532 nm continuous wave laser (Genesis MX STM-Series), with a beam diameter of 1 mm and a maximum power of 1 W, was used as a monochromatic light source. Without further tuning of the beam width, the laser is termed the 'spotlight' as it shines on samples with a smaller diameter of illumination. A beam expander (10×) was used to expand the laser beam diameter to 10 mm, which is termed the 'area light'. A white light source equipped with a collimator was designed and fabricated to serve as a broadband light source (50 mm in diameter with a maximum power of 1 W). The SunBOT was immersed in a water bath inside a glass container with a precise temperature control (0.1 °C precision). An optical power meter (Newport 1830-C) was used to calibrate the power output of the light sources. The real-time azimuth-angle variation was performed by rotating a rotation stage on which the SunBOT was placed on its concentric point. The light sources were fixed and shone on the SunBOT with different zenith angles. All the photos and videos were recorded by a camera (Olympus E-M10). Detailed characterizations are given in Supplementary Section 2.

Characterization of the omnidirectional SVG. The SunBOT array (5 × 7) was designed to contain micropillars 300 μm in diameter and 1 mm in height with a 700 μm spacing. The pillars became wider (500 μm in diameter and 500 μm in spacing) after washing off the solvent DMSO with water. The SunBOT array with a 70% filling ratio was fabricated by the same method, but with a different mould. The SunBOT array was maintained floating at the water/air interface of a water reservoir inside a container placed on a precision scale (USS-DBS8).

The light sources were illuminated on the SunBOT array with different oblique angles. The vapour generation was characterized by the mass reduction recorded by the precision scale. A detailed characterization method is given in Supplementary Section 3.

Simulation. The light tracking of the hydrogel pillar of the SunBOT is a transient multiphysics process that mainly involves a mass diffusion of water into and/or out of the gel, a large deformation of the gel network and a heat-transfer process. To model this complicated behaviour, the nonlinear field theory that couples large deformation and mass diffusion and heat transfer theory were used and implemented in the environment of commercial multi-physics modelling software COMSOL. Details of the simulation methods are given in Supplementary Section 4.

Data availability
The data that support the plots within this paper and other findings of this study are available from the corresponding author upon reasonable request.

Author contributions
X.H. conceived the concept, planned the project and supervised the research. X.H., X.Q., Y.Z., Y.A. and H.G. designed and conducted the experiments and data analysis. X.Q., Y.Z., Y.A., M.H., Y.Y., H.G. and J.C. conducted the fabrication of various SunBOTs and SVG characterization. N.L. synthesized the AuNPs. X.W., H.J., T.G. and L.P. developed the model and numerical code and carried out the computational simulations. X.H., X.Q., Y.Z., Y.A., H.J., L.T. and M.M. wrote the manuscript. X.Q., Y.Z. and Y.A. contributed to the work equally.

Competing interests
The authors declare no competing interests.

Additional information
Supplementary information is available for this paper at https://doi.org/10.1038/s41565-019-0562-3.

Correspondence and requests for materials should be addressed to X.H.

Reprints and permissions information is available at www.nature.com/reprints.